Updated High-Temperature Opacities for The Dartmouth Stellar Evolution Program and their Effect on the Jao Gap Location

Thomas M. Boudreaux[1] and Brian C. Chaboyer[1]

[1]*Department of Physics and Astronomy, Dartmouth College, Hanover, NH 03755, USA*

ABSTRACT

The Jao Gap, a 17 percent decrease in stellar density at $M_G \sim 10$ identified in both Gaia DR2 and EDR3 data, presents a new method to probe the interior structure of stars near the fully convective transition mass. The Gap is believed to originate from convective kissing instability wherein asymmetric production of He^3 causes the core convective zone of a star to periodically expand and contract and consequently the stars' luminosity to vary. Modeling of the Gap has revealed a sensitivity in its magnitude to a population's metallicity primarily through opacity. Thus far, models of the Jao Gap have relied on OPAL high-temperature radiative opacities. Here we present updated synthetic population models tracing the Gap location modeled with the Dartmouth stellar evolution code using the OPLIB high-temperature radiative opacities. Use of these updated opacities changes the predicted location of the Jao Gap by ~ 0.05 mag as compared to models which use the OPAL opacities.

Keywords: Stellar Evolution (1599) — Stellar Evolutionary Models (2046)

1. INTRODUCTION

Jao et al. (2018) discovered a novel feature in the Gaia $G_{BP} - G_{RP}$ color-magnitude-diagram. Around $M_G = 10$ there is an approximately 17% decrease in stellar density of the sample of stars Jao et al. considered. Subsequently, this has become known as either the Jao Gap, or Gaia M dwarf Gap. Section ?? will go into more detail regarding the physics underpinning this feature; however, in brief convective instabilities in the core are believed to form for stars straddling the fully convective transition mass (0.3 - 0.35 $M_\odot$) (Baraffe & Chabrier 2018). These instabilities interupt the normal, slow, main sequence luminosity evolution of a star and resulting in lower than expected luminosities [WORD-ING] (Jao & Feiden 2020).

The Jao Gap, inherently a feature of M dwarf populations, provides an enticing and unique view into the interior physics of these stars (Feiden et al. 2021). This is especially important as, unlike more massive stars, M dwarf seismology is currently infeasible due to the short periods and extremely small magnitude's which both ra-

Corresponding author: Thomas M. Boudreaux

thomas.m.boudreaux.gr@dartmouth.edu,
thomas@boudreauxmail.com

dial and low-order low-degree non-radial seismic waves are predicted to have in such low mass stars (Rodríguez-López 2019). The Jao Gap therefore provides one of the only current methods to probe the interior physics of M dwarfs.

Stellar modeling has been successful in reproducing the Jao Gap (e.g. Feiden et al. 2021; Mansfield & Kroupa 2021) and, with these models, we have begun to understand which parameters constrain the Jao Gap's location. For example, it is now well documented that metallicity affects the Jao Gap's color, with higher metallicity stellar populations showing the Jao Gap at consistently higher masses / bluer colors (Mansfield & Kroupa 2021).

2. JAO GAP

A theoretical explanation for the Jao Gap (Figure 1) comes from van Saders & Pinsonneault (2012), who propose that in a star directly above the transition mass, due to asymmetric production and destruction of He^3 during the proton-proton I chain (ppI), periodic luminosity variations can be induced. This process is known as convective-kissing instability. Such a star will descend the pre-main sequence with a radiative core; however, as the star reaches the zero age main sequence (ZAMS) and as the core temperature exceeds 7×10^6 K, enough energy will be produced by the ppI chain that the core becomes convective. At this point the star exists with
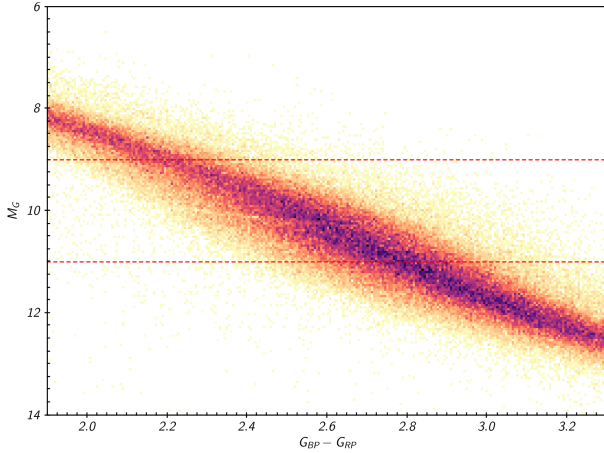
Figure 1. Figure 1 from Jao et al. (2018) showing the so called "Jao Gap" at $M_G \approx 10$ [SHOULD I REMAKE THIS USING DR3 DATA?]

both a convective core and envelope, in addition to a thin, radiative, layer separating the two. Subsequently, asymmetries in ppI affect the evolution of the star's convective core.

The proton-proton I chain constitutes three reactions

1. $p + p \longrightarrow d + e^+ + \nu_e$

2. $p + d \longrightarrow {}^3\text{He} + \gamma$

3. ${}^3\text{He} + {}^3\text{He} \longrightarrow {}^3\text{He} + 2p$

Because reaction 3 of ppI consumes ^{3}He at a slower rate than it is produced by reaction 2, ^{3}He abundance increases in the core increasing energy generation. The core convective zone will therefore expand as more of the star becomes unstable to convection. This expansion will continue until the core connects with the convective envelope. At this point convective mixing can transport material throughout the entire radius of the star and the high concentration of ^{3}He will rapidly diffuse outward, away from the core, again decreasing energy generation as reaction 3 slows down. Ultimately, this leads to the convective region around the core pulling back away from the convective envelope, leaving in place the radiative transition zone, at which point ^{3}He concentrations build up in the core until it once again expands to meet the envelope. This process repeats until the He^3 concentration throughout the star is enough such that the core can sustain nuclear reaction rates which keep it in with the envelope, resulting in a fully convective star.

2.0.1. *Modeling the Gap*

Since the identification of the Gaia M-dwarf gap, stellar modeling has been conducted to better constrain its location, effects, and exact cause. Both Mansfield &

Kroupa (2021) and Feiden et al. (2021) identify that the gap's mass location is correlated with model metallicity — the mass-luminosity discontinuity in lower metallicity models being at a commensurately lower mass. Feiden et al. (2021) suggests this dependence is due to the steep relation of the radiative temperature gradient, ∇_{rad}, on temperature and in turn, on stellar mass.

$$\nabla_{rad} \propto \frac{L\kappa}{T^4} \tag{1}$$

As metallicity decreases so does opacity, which, by Equation 1, dramatically lowers the temperature where radiation will dominate energy transport (Chabrier & Baraffe 1997). Since main sequence stars are virialized the core temperature is proportional to the core density and total mass (Equation 2). Therefore, if the core temperature where convective-kissing instability is expected decreases with metallicity, so too will the mass of stars which experience such instabilities.

$$T_c \propto \rho_c M^2 \tag{2}$$

This strong opacity dependence presents a slight problem where modeling is concerned. With current computational tools it is infeasible to compute opacities on the fly; rather, Rossland Mean opacity (κ_R) for individual elements must be pre-tabulated over a wide range of temperatures and densities. These opacities can then be somewhat arbitrarily mixed together and interpolated to form opacity lookup-tables. Multiple groups have performed these calculations and subsequently made tables available to the wider community, these include the Opacity Project (OP Seaton et al. 1994), Laurence Livermore National Labs OPAL opacity tables (Iglesias & Rogers 1996), and Los Alamos National Labs OPLIB opacity tables (Colgan et al. 2016).

3. UPDATED OPACITIES

OPAL high-temperature radiative opacity tables in particular are very widely used by current generation stellar evolution programs (in addition to current generation stellar model and isochrone grids). However, there are two primary issues with these tables, one, they are relativly old and therefore do not incorperate the most up to date understanding of plasma modeling in their code [CITATION], and two, they report rossland mean opacitieis to only N digits [WHICH IS AN ISSUE WHY?].

While the two issues given above should have relativly small affects, the strong theoretical opacity dependence of the Jao Gap raises the potential for these small effects

Z =	Z$_\odot$	0.01	0.001	0.0001
OPAL	0.3803 - 0.384	0.3583 - 0.3631	0.34 - 0.3448	0.362 - 0.3663
OPLIB	0.374 - 0.3767	0.3526 - 0.3567	0.3358 - 0.3406	0.3577 - 0.3621

Table 1. Mass ranges for the discontinuity in OPAL and OPLIB models. Masses are given in solar masses.
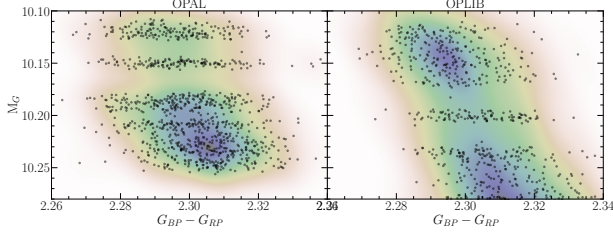

Figure 2. Synthetic CMDs derived from simple population synthesis code. (Left) CMD showing the Jao Gap for a GS98 composition stellar population generated from models evolved using OPAL opacity tables. (Right) CMD showing the Jao Gap for a GS98 stellar population generated from models evolved using the OPLIB opacity tables. Note how the OPLIB derived Jao Gap is slightly brighter than the OPAL Jao Gap.

to measurably shift the gap's location. In order to address both the out of date plasma modeling and the low numeric presicion we update DSEP to use high temperature opacity tables based on measurements from Los Alamos national Labs T-1 group (OPLIB, Colgan et al. 2016). The OPLIB tables use the much more up-to-date ATOMIC plasma modeling code [CITATION] in addition to reporting rossland mean opacities to N digits of numeric presicion.

Los Alamos National Labs OPLIB opacity tables were first computed in the 1990s using the LEDCOP code (Magee et al. 1995); however, since 2004 efforts have been underway to shift OPLIP from LEDCOP to ATOMIC (Magee et al. 2004). ATOMIC is a LTE and non-LTE opacity and plasma modeling code. A major strength of ATOMIC when compared to the older LEDCOP is its ability to vary its refinement level (Fontes et al. 2015). For a more detailed breakdown of how the most up-to-date set of OPLIB tables are generated see (Colgan et al. 2016).

The most up to date OPLIB tables include monochromatic Rosseland mean opacities for elements hydrogen through zinc over temperatures 0.5eV to 100 keV and for mass densities from approximately 10^{-8} g cm^{-3} up to approximately 10^{4} g cm^{-3} (though the exact mass density range varies as a function of temperature). The Rosseland mean opacity as reported in OPLIB tables is given in Equation 3.
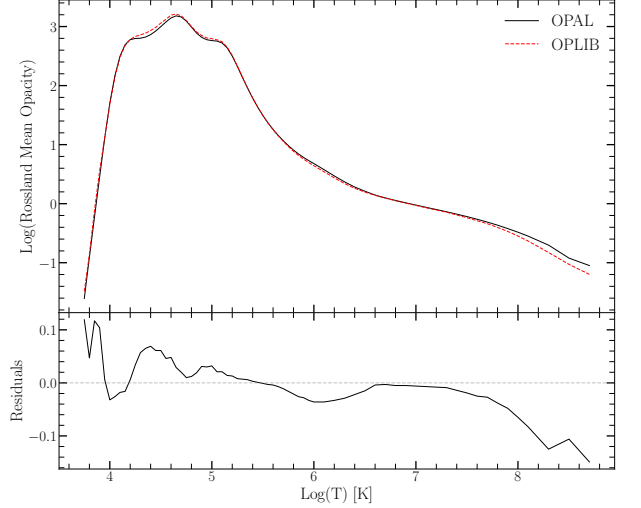
Figure 3. Rossland Mean Opacity from both OPAL (black solid) and OPLIB (red dashed) for a GS98 solar composition. Note how above 10^6 K OPLIB opacities are uniformly smaller than those from OPAL.

$$\frac{1}{\kappa_R} = \frac{\int_0^\infty \frac{1}{\kappa_\nu} n_\nu^3 \frac{\partial B_\nu}{\partial T} d\nu}{\int_0^\infty \frac{\partial B_\nu}{\partial T} d\nu} \quad (3)$$

Here, B_ν is the Planck function, n_ν is the frequency-dependent refractive index (Armstrong et al. 2014), and κ_ν is the frequency-dependent opacity. κ_ν is defined as the sum of the bound-bound, bound-free, free-free, and scattering opacity computed by ATOMIC.

When comparing OPAL and OPLIB opacity tables (Figure 3) we find OPLIB opacities are systematically lower than OPAL opacities for temperature above 10^6 K (Figure 3). These lower opacities will result the temperature where radiation dominates energy transport lowering [CITATION?]. Consequently, the radiative layer in stellar models evolved using OPLIB opacity tables will be [further?] out from the models center than it would be in models making use of OPAL tables.

3.1. Table Querying and Conversion

DSEP uses pre-computed high-temperature opacity tables, in the format supplied by OPAL. These tables list the Rosseland-mean opacity, κ_R, along three dimensions: temperature, a density proxy R, and composition. R is defined as

$$R = \frac{\rho}{T_6^3} \quad (4)$$

Where $T_6 = T \times 10^{-6}$ and ρ is the mass density. If T and ρ are given in cgs then for much of the radius of a star $\log(R) \sim -1.5$. R is used, as opposed to simply tracking opacity over density, as R stays relatively fixed throuhout the radius of most main sequence stars, whereas there is an enormous dynamic range of densities within a star ($\sim 10^5$ [g cm^{-3}] at the core of an RGB star all the way down to $\sim 10^{-8}$ [g cm^{-3}] within the envelope).

OPLIB tables are queried from a web interface[1]. In order to generate many tables easily and quickly we develop a web scraper built with Python's `requests` module in addition to the 3rd party `mechanize` and `BeautifulSoup` modules (Chandra & Varanasi 2015; Richardson 2007) which can get tables with minimal intervention. This web scraper submits a user requested chemical composition (composed of mass fractions for elements from Hydrogen to Zinc) to the Los Alamos web form, selects 0.0005 keV as the lower temperature bound and 60 keV as the upper temperature bound, and finally requests opacity measurements for 100 densities, ranging from $1.77827941 \times 10^{-15}$ [g cm^{-3}] up to 1×10^7 [g cm^{-3}], at each temperature interval. These correspond to approximately the same temperature and density range of opacities present in the OPAL opacity tables.

OPLIB reports κ_R as a function of mass density, temperature in keV, and composition. Recall that DSEP accepts tables where opacity is given as a function of temperature in Kelvin, R, and composition. The conversion from temperature in keV to Kelvin is trivial

$$T_K = T_{keV} * 11604525.0061657 \qquad (5)$$

However, the conversion from mass density to R is more involved. Because R is coupled with both mass density and temperature there there is no way to directly convert tabulated values of opacity reported in the OPLIB tables to their equivalents in R space. Instead we must rotate the tables, interpolating $\kappa_R(\rho, T_{eff}) \rightarrow \kappa_R(R, T_{eff})$.

To preform this rotation we use the `interp2d` function within `scipy`'s `interpolate` (Virtanen et al. 2020) module to construct a cubic bivariate B-spline (DIERCKX 1981) interpolating function s, with a smoothing factor of 0, representing the surface $\kappa_R(\rho, T_{eff})$. For each R^i and T_{eff}^j which DSEP expects high-temperature opacities to be reported for, we evaluate Equation 4 to find $\rho^{ij} = \rho(T_{eff}^j, R^i)$. Opacities in T_{eff}, R space are then inferred as $\kappa_R^{ij}(R^i, T_{eff}^j) = s(\rho^{ij}, T_{eff}^j)$.

[1] https://aphysics2.lanl.gov/apps/
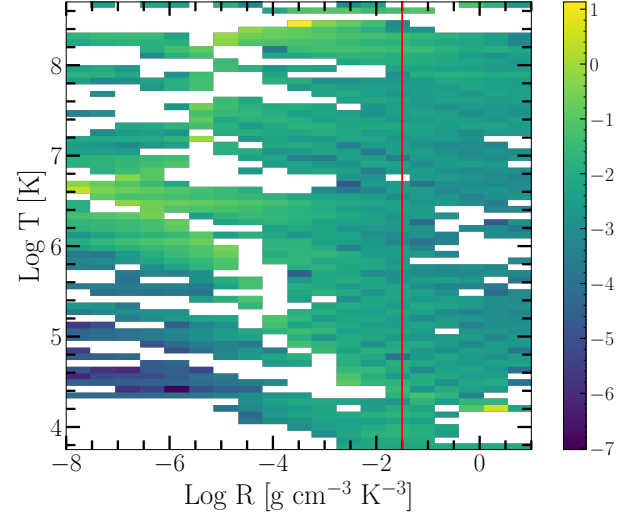
Figure 4. Log Fractional Difference between opacities in $\kappa_R(\rho, T_{eff})$ space directly queried from the OPLIB webform and those which have been interpolated into $Log(R)$ space and back. Note that, due to the temperature grid DSEP uses not aligning perfectly which the temperature grid OPLIB uses there may be edge effects where the interpolation is poorly constrained. The red line corresponds to $Log(R) = -1.5$ where much of a stellar model's radius exists.

As first-order validation of this interpolation scheme we can preform a similar interpolation in the opposite direction, rotating the tables back to $\kappa_R(\rho, T_{eff})$ and then comparing the initial, "raw", opacities to those which have gone through the interpolations process. Figure 4 shows the fractional difference between the raw opacities and a set which have gone through this double interpolation. The red line denotes $Log(R) = -1.5$ where models will tend to sit for much of their radius. Along the $Log(R) = -1.5$ line the mean fractional difference is $\langle \delta \rangle = 0.006$ with an uncertainty of $\sigma_{\langle \delta \rangle} = 0.009$. One point of note is that, because the initial rotation into $Log(R)$ space also reduces the domain of the opacity function interpolation-edge effects which we avoid initially by extending the domain past what DSEP needs cannot be avoided when interpolating back into ρ space. [IS THERE SOME MORE CLEAR VALIDATION WHICH I SHOULD PREFORM?]

3.2. Opacity Validation

In order to further validate the OPLIB high-temperature opacities we first visually compare a set of opacity vs. temperature curves from OPLIB at a constant R and Grevesse & Sauval (1998) composition (GS98) to the same curve from OPAL. A characteristic opacity vs temperature curve is shown in Figure 5, $\log_{10}(R) = -1.5$ is chosen as for much of the radius of a main sequence star $\log_{10}(R)$ is around that value.
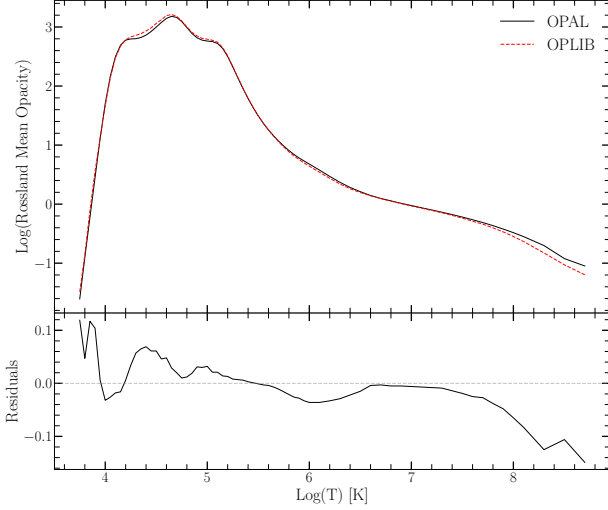
Figure 5. Rosseland mean opacity with the GS98 solar composition for both OPAL opacities and OPLIB opacities (top). Residuals between OPLIB opacities and OPAL opacities (bottom). These opacities are plotted at $\log_{10}(R) = -1.5$, $X = 0.7$, and $Z = 0.02$.

The largest variation in κ_R from OPAL to OPLIB at $\log_{10}(R) = -1.5$ is on the order of a few percent. This is inline with expectations of OPLIB and OPAL being in relatively close agreement (Colgan et al. 2016).

To further validate the OPLIB opacities we generate a solar calibrated stellar model (SCSM) using the new tables. SCSMs are generally models where some initial parameters have been iteratively adjusted to minimize some loss function between that models output parameters and the observed values of those parameters for the Sun. In the context of this paper we adjust both the convective mixing length parameter, α_{ML}, and the initial Hydrogen mass fraction, X, to minimize the difference between the models final radius and luminosity and that of the sun.

Optimization of α_{ML} and X is done with a quite naive gradient descent algorithm. For each optimization step three models are evolved: a reference model, a model with a small perturbation to the hydrogen mass fraction but the same mixing length as the reference model, and a model with a small perturbation to the mixing length but the same hydrogen mass fraction as the reference. Perturbations are sampled from a normal distribution (implemented though `numpy.random`) with scale set to an adjustable parameter, η. This distribution is sampled and that sample is then added to the reference value for either X or α_{ML}. The luminosity and radius of the three evolved models are compared to solar values and the gradient of the resultant $L - L_\odot$, $R - R_\odot$ surface is followed down to new estimates for the reference values of X and α_{ML}. This process is is repeated until the
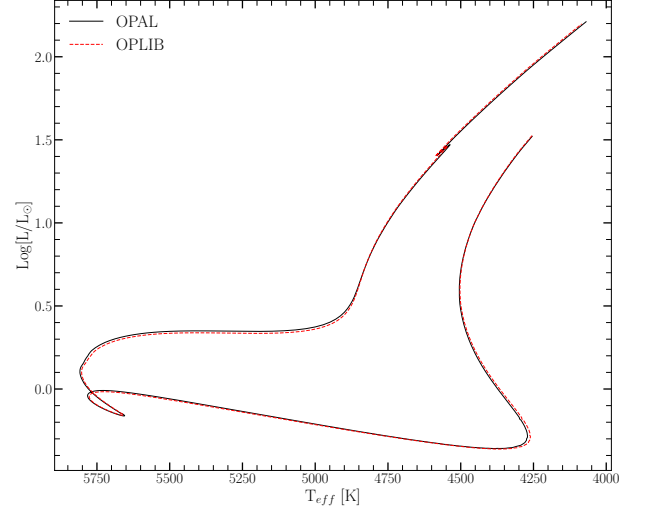
Figure 6. HR Diagram for the two SCSMs, OPAL and OPLIB. OPLIB is show as a grey dashed line.

difference between successive X and α_{ML} drops below one part in 10^5.

If we generate a SCSM using the GS98 OPAL opacity tables we find a best estimate of $X = 0.7066$ and $\alpha_{ML} = 1.9333$. When we preform the same calibration but substituting in the GS98 OPLIB tables we find $X = 0.7107$ and $\alpha_{ML} = 1.9629$. This represents $\sim 0.5\%$ difference in the SCSM hydrogen mass fractions and $\sim 1.5\%$ change in the SCSM convective mixing length parameters when comparing models using OPAL and OPLIB tables. An HR-diagram for the two calibrated models is presented in Figure 6. While the two evolutionary tracks are very similar, note that the OPLIB SCSM's luminosity is systematically lower at the same effective temperature all the way from the premain sequence up and until the star leaves the main sequence, at which point it is effectively the same as the OPAL SCSM. This luminosity difference between OPAL and OPLIB based models is consistent with expectations given the differences in opacities. Opacity is of primary importance only in radiative regions of a star ($\gtrsim 10^6$ K). Figure 5 shows that OPLIB opacities are uniformly lower than OPAL opacities above 10^6 K. These lower opacities will steepen the temperature gradient within the stellar model as radiation streams more freely outward.

4. MODELING

In order to address the two main issues with using OPAL opacity tables we use our OPLIB opacity table web scraper to generate a set of tables that consistently model lower metallicities. Specifically, we generate tables for $Z_\odot = 0.017$, $Z = 0.01$, $Z = 0.001$, and $Z = 0.0001$. Compositions are derived from the GS98

solar composition, with the mass fractions between metals remaining constant, and only the total metal mass fraction is allowed to vary. Moreover, Helium mass fraction is held constant as extra mass from the reduced metallicity is put into additional Hydrogen.

For each metallicity 101, uniformly spaced, models from 0.3 to 0.5 $M_\odot$ (spacing of 0.001 $M_\odot$) are evolve with both the GS98 OPAL opacity table and OPLIB tables, hereafter these are the "coarse" models. For each set of coarse models the discontinuity in the mass-luminosity relation is identified at an age of 7 Gyr (Figures ?? & ?? shows a characteristic example).

Immediately, the difference in mass where the discontinuity manifests is clear. For each metallicity the discontinuity in the OPLIB models is approximately one one-hundredth of a solar mass lower than the discontinuity in the OPAL models. We can validate that this discontinuity is indeed correlated with the convective transition mass; Figure 7 shows an example of the model forming radiative zones at approximately the same masses where the discontinuity in the mass-luminosity function exists.

At this resolution only a few models exist within the mass range of the discontinuity. In order to better constrain its location we run a series of "fine" models, with a mass step of 0.0001 $M_\odot$ and ranging from where the mass derivative first exceeds two sigma away from the mean derivative value up to the mass where it last exceeds two sigma away from the mean. A characteristic fine mass-luminosity relation is shown in Figure 8.

Using the fine models we identify the location of the discontinuity in the same manner as before, results of this are presented in Table 1. Of note with the mass ranges we measure for the discontinuity is that are generally not in agreement with those measured in Mansfield & Kroupa (2021). However, the luminosity difference from over the gap ($\approx 0.1 mag$) is similar to both the observational difference and that reported in Mansfield & Kroupa (2021). Currently, it is not clear why our mass range is not in agreement with the Mansfield & Kroupa (2021) mass range and further investigation is therefore needed.

5. RESULTS

6. CONCLUSION

REFERENCES

Armstrong, G. S. J., Colgan, J., Kilcrease, D. P., & Magee, N. H. 2014, High Energy Density Physics, 10, 61, doi: 10.1016/j.hedp.2013.10.005

Baraffe, I., & Chabrier, G. 2018, A&A, 619, A177, doi: 10.1051/0004-6361/201834062

Chabrier, G., & Baraffe, I. 1997, A&A, 327, 1039. https://arxiv.org/abs/astro-ph/9704118

Chandra, R. V., & Varanasi, B. S. 2015, Python requests essentials (Packt Publishing Ltd)

Colgan, J., Kilcrease, D. P., Magee, N. H., et al. 2016, in APS Meeting Abstracts, Vol. 2016, APS Division of Atomic, Molecular and Optical Physics Meeting Abstracts, D1.008

DIERCKX, P. 1981, IMA Journal of Numerical Analysis, 1, 267, doi: 10.1093/imanum/1.3.267

Feiden, G. A., Skidmore, K., & Jao, W.-C. 2021, ApJ, 907, 53, doi: 10.3847/1538-4357/abcc03

Fontes, C. J., Zhang, H. L., Abdallah, J., J., et al. 2015, Journal of Physics B Atomic Molecular Physics, 48, 144014, doi: 10.1088/0953-4075/48/14/144014

Grevesse, N., & Sauval, A. J. 1998, SSRv, 85, 161, doi: 10.1023/A:1005161325181

Iglesias, C. A., & Rogers, F. J. 1996, ApJ, 464, 943, doi: 10.1086/177381
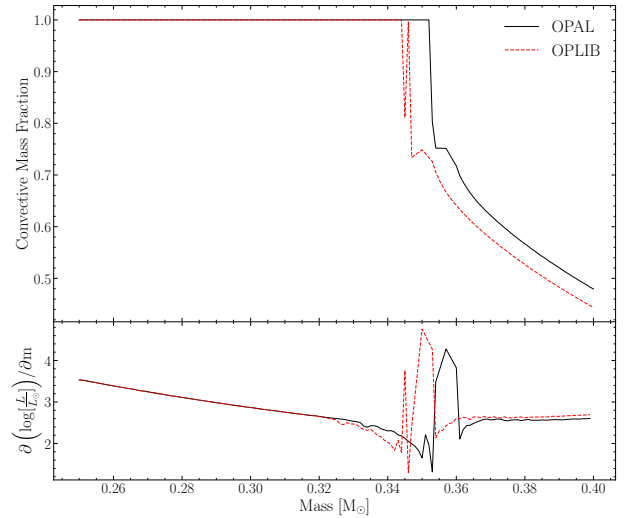
Figure 7. Convective Mass Fraction vs. initial model mass for Z=0.01 at 7 Gyr (top), Derivative of luminosity with respect to mass for the OPAL and OPLIB models (bottom). Note how the model transitions from fully convective at approximately the same mass where the discontinuity exists.

Jao, W.-C., & Feiden, G. A. 2020, AJ, 160, 102, doi: 10.3847/1538-3881/aba192
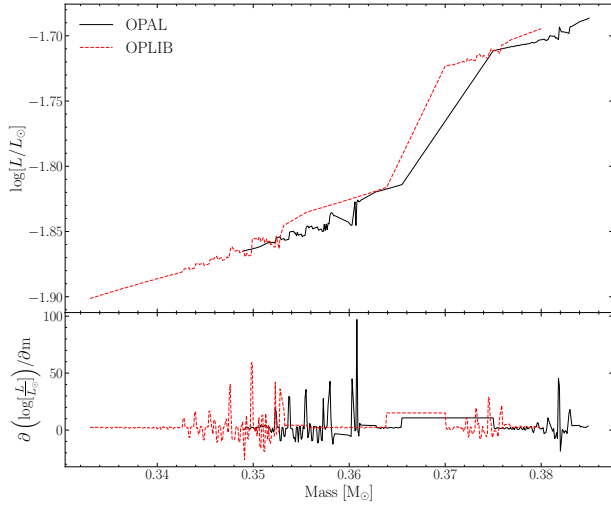
Figure 8. Mass-Luminosity relation for Z=0.01 at 7 Gyr for models run with both OPAL and OPLIB high-temperature opacity tables and a mass step between them of 0.0001 $M_\odot$ (top). Derivative of luminosity with respect to mass for the OPAL and OPLIB models (bottom).

Jao, W.-C., Henry, T. J., Gies, D. R., & Hambly, N. C. 2018, ApJL, 861, L11, doi: 10.3847/2041-8213/aacdf6

Magee, N. H., Abdallah, J., J., Clark, R. E. H., et al. 1995, in Astronomical Society of the Pacific Conference Series, Vol. 78, Astrophysical Applications of Powerful New Databases, ed. S. J. Adelman & W. L. Wiese, 51

Magee, N. H., Abdallah, J., Colgan, J., et al. 2004, in American Institute of Physics Conference Series, Vol. 730, Atomic Processes in Plasmas: 14th APS Topical Conference on Atomic Processes in Plasmas, ed. J. S. Cohen, D. P. Kilcrease, & S. Mazavet, 168–179

Mansfield, S., & Kroupa, P. 2021, A&A, 650, A184, doi: 10.1051/0004-6361/202140536

Richardson, L. 2007, April

Rodríguez-López, C. 2019, Frontiers in Astronomy and Space Sciences, 6, 76, doi: 10.3389/fspas.2019.00076

Seaton, M. J., Yan, Y., Mihalas, D., & Pradhan, A. K. 1994, MNRAS, 266, 805, doi: 10.1093/mnras/266.4.805

van Saders, J. L., & Pinsonneault, M. H. 2012, ApJ, 751, 98, doi: 10.1088/0004-637X/751/2/98

Virtanen, P., Gommers, R., Oliphant, T. E., et al. 2020, Nature Methods, 17, 261, doi: 10.1038/s41592-019-0686-2